

# FORCE RIPPLE COMPENSATOR FOR A VECTOR CONTROLLED PM LINEAR SYNCHRONOUS MOTOR

Markus Hirvonen and Heikki Handroos

*Institute of Mechatronics and Virtual Engineering, Lappeenranta University of Technology, Lappeenranta, Finland*

Olli Pyrhönen

*Department of Electrical Engineering, Lappeenranta University of Technology, Lappeenranta, Finland*

**Keywords:** Cogging, Disturbance Observation, Linear Motor, Velocity Control, Vibration Suppression.

**Abstract:** A dynamic model including non-idealities for a permanent magnet linear synchronous motor (PMLSM) is postulated and verified. The non-idealities acting on the physical linear motor are measured and analyzed. These experimental results are utilized in the model. The verified simulation model is used in developing a force disturbance compensator for the velocity controller of the motor. The force non-idealities, such as the cogging force, friction and load force variation, are estimated using a disturbance observer. The acceleration signal in the observer is derived through the use of a low-acceleration estimator. The significant effects of the disturbance compensator on the simulated and measured dynamics of the motor are shown.

## 1 INTRODUCTION

The linear motor is an old invention but it is only recently that, as a result of the development of permanent magnets and their decreased costs, permanent magnet linear motors have become a viable alternative to rotating motors fitted with linear transmissions. In machine automation, linear movement has traditionally been transmitted from a rotary actuator by means of a ball screw, rack and pinion or belt. The linear motor simplifies the mechanical structure, eliminating the contact-type nonlinearities caused by backlash, friction, and compliance. In addition, the main benefits of a linear motor include its high-power density, reliability and efficiency.

Nowadays, the controllers commercially available, mainly PID algorithms with fixed gains, are unable to compensate for the undesirable phenomena that reduce the precision of motion such as backlash, static friction, load variations etc. Large controller gains are needed in order to maintain the stiff control required when suppressing load disturbances that tend to reduce the stability of a system. Therefore, extended methods for the compensation of disturbance have become an

important topic of research. By compensating for an unknown time-varying force based on the estimation of such a force, faster speed responses and smaller speed ripples can be achieved.

In disturbance compensation, the compensation technique itself is a very simple feed-forward control, but the difference arises from the different disturbance estimation algorithms. In (Castillo-Castaneda *et al.*, 2001), the friction compensation has been studied using model-based estimation. One disadvantage of this technique is that it is suitable for tracking only, since the desired velocity must be known in advance. Kim *et al.* (2002) and Tan *et al.* (2002) have studied sliding mode estimators in compensation feedback, while Godler *et al.* (1999), Deur *et al.* (2000), Bassi *et al.* (1999) and Hong *et al.* (1998) have studied the disturbance observer of a more general algorithm. Godler *et al.* (1999) compared load disturbance compensation with an acceleration control loop inside a speed loop. They have found that control implemented using an acceleration control loop can better tolerate parameter variation as well as disturbance in comparison to robust control with a disturbance observer. On the other hand, Deur *et al.* (2000) suggested the use of a disturbance observer in industrial applications due to its simple

implementation as well as simple design which has no robustness constraints.

The motor model discussed in the above-mentioned papers is a simplified model. The development of computers and software has made it feasible to simulate the more detailed dynamical behavior of machine systems. This paper discusses the use of a more detailed non-linear dynamic model for the analysis of a linear transmission system. The motor studied in this paper is a commercial three-phase linear synchronous motor application. The moving part (the mover) consists of a slotted armature and a three phase windings, while the surface permanent magnets (the SPMs) are mounted along the whole length of the path (the stator).

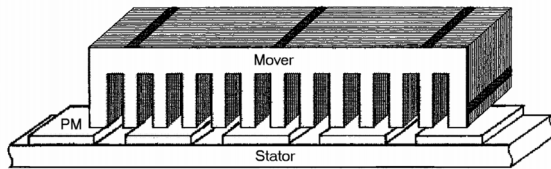


Figure 1: The structure of the studied linear motor.

First of all, the equations for modelling the vector-controlled motor drive and non-idealities are derived. Then, the simulation model is verified with the measurements from physical linear motor applications, and the comparison of the responses is shown in the study. Finally, a disturbance observer based on (Hong *et al.*, 1998), (Godler *et al.*, 1999), (Deur *et al.*, 2000), and (Bassi *et al.*, 1999) is implemented in the physical motor system after being tested in the simulation model, and the results and conclusions are presented.

## 2 SIMULATION MODEL

### 2.1 Model of LSM

The modeling of the dynamics of the linear synchronous motor examined in this paper is based on the space-vector theory. The time-varying parameters are eliminated and all the variables expressed on orthogonal or mutually decoupled direct and quadrature axes, which move at a synchronous speed of  $\omega_s$ . The d- and q-axes equivalent to the circuit of the PMLSM are shown in figure 2, and the corresponding equations are (1) and (2), respectively.

The voltage equations for the synchronous

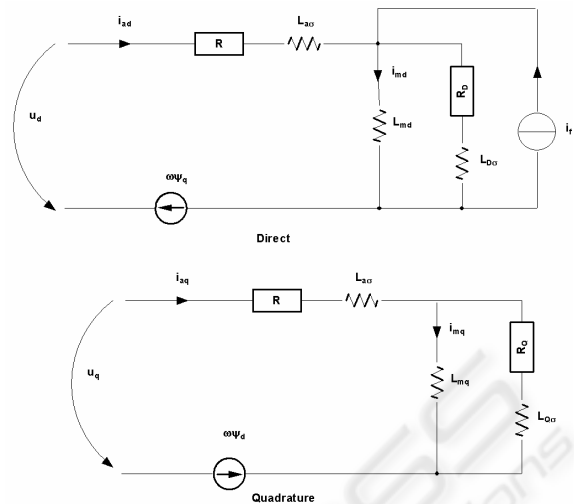


Figure 2: Two axial models of the linear synchronous motor.

machines are

$$u_d = Ri_{ad} + \frac{d\psi_{ad}}{dt} - \omega_s \psi_q \quad (1)$$

$$u_q = Ri_{aq} + \frac{d\psi_{aq}}{dt} + \omega_s \psi_d \quad (2)$$

where  $u_d$  and  $u_q$  are the d- and q-axis components of the terminal voltage,  $i_{ad}$  and  $i_{aq}$  the d- and q-axis components of the armature current,  $R$  is the armature winding resistance and  $\psi_d$ ,  $\psi_q$  are the d- and q-axis flux linkage components of the armature windings. The synchronous speed can be expressed as  $\omega_s = \pi v_s / \tau$ , where  $v_s$  is the linear synchronous velocity and  $\tau$  the pole pitch. Although the physical system does not contain a damper, which in PMLSM usually takes the form of an aluminum cover on the PMs, virtual damping must be included in the model, due to eddy currents. The voltage equations of the short-circuited damper winding are

$$0 = R_D i_D + \frac{d\psi_D}{dt} \quad (3)$$

$$0 = R_Q i_Q + \frac{d\psi_Q}{dt} \quad (4)$$

where  $R_D$  and  $R_Q$  are the d- and q-axis components of the damper winding resistance and  $i_D$  and  $i_Q$  the d- and q-axis components of the damper winding current. The armature and damper winding flux linkages in the above equations are

$$\psi_d = L_{ad}i_{ad} + L_{md}i_D + \psi_{pm}, \quad (5)$$

$$\psi_q = L_{aq}i_{aq} + L_{mq}i_Q, \quad (6)$$

$$\psi_D = L_{md}i_{ad} + L_D i_D + \psi_{pm}, \quad (7)$$

$$\psi_Q = L_{mq}i_{aq} + L_Q i_Q, \quad (8)$$

where  $L_{ad}$  and  $L_{aq}$  are the d- and q-axis components of the armature self-inductance,  $L_D$  and  $L_Q$  the d- and q-axis components of the damper winding inductance,  $L_{md}$  and  $L_{mq}$  the d- and q-axis components of the magnetizing inductance and  $\psi_{pm}$  is the flux linkage per phase of the permanent magnet. By solving the flux linkage differential equations from (1) to (4) and substituting the current equations from (5) to (8) into these equations, the equations for the simulation model of the linear motor can be derived. The electromagnetic thrust of a PMLSM is (Morimoto *et al.*, 1997)

$$F_{dx} = \frac{p_e}{v_s} = \frac{\pi}{\tau} (\psi_d i_{aq} - \psi_q i_{ad}), \quad (9)$$

where  $p_e$  is the electrical power.

## 2.2 Non-idealities of PMLSM

The force ripple of the PMLSM is larger than that of rotary motors because of the finite length of the stator or mover and the wide slot opening. In the PMLSM, the thrust ripple is caused mainly by the detent force generated between the PMs and the armature. This type of force can be divided into two components, for tooth- and core-type detent force. In the tooth detent force, the force component is generated between the PMs and the primary teeth, while the core-type detent force component is generated between PMs and the primary core. The wavelength of the core component is usually one pole pitch, while that of the teeth component is one slot pitch. The core-type detent force can be efficiently reduced by optimizing the length of the moving part or smooth-forming the edges of the mover, and the tooth-type detent force can be reduced by skewing the magnets and chamfering the edges of the teeth (Jung *et al.*, 2002), (Hyun *et al.*, 1999), (Inoue *et al.*, 2000), (Zhu *et al.*, 1997), (Hor *et al.*, 1998).

The detent force effect tends to move the mover

to a position in which the energy of the magnetic circuit is at its minimum. This phenomenon attempts to stall the mover at the stator pole positions and is always present, even when no current is flowing through the motor coils (Otten *et al.*, 1997). The ripple of the detent force produces both vibrations and noise and reduces controllability (Chun *et al.*, 2000). The force ripple is dominant at low velocities and accelerations. At higher velocities, the cogging force is relatively small and the influence of dynamic effects (acceleration and deceleration) is more dominant (Otten *et al.*, 2000). In this study, the detent force was measured in the reference system. The force ripple can be described by sinusoidal functions of the load position,  $x$ , with a period of  $\varphi$  and an amplitude of  $A_r$ , i.e.,

$$F_{ripple} = A_{r1} \sin(\varphi_1 x) [A_{r1} + A_{r2} \sin(\varphi_2 x)]. \quad (10)$$

In figure 3, the results of the simulation are compared with those measured in the reference system.

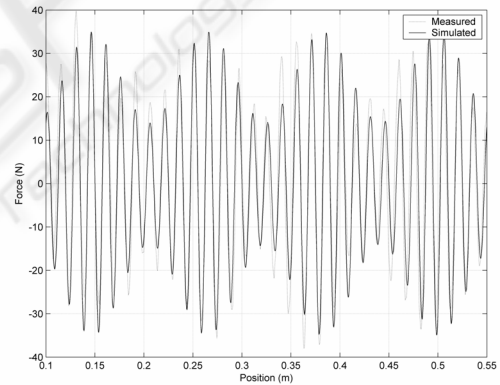


Figure 3: Comparison of measured and simulated detent forces.

The reluctance force is another phenomenon that occurs in linear synchronous motors. A lot of research has been carried out into the reluctance in linear induction machines, in which the phenomenon depends on velocity. The reluctance force in PMLSMs has been studied to a lesser extent. The reluctance force is due to the variations in the self-inductance of the windings with respect to the relative position between the mover and the magnets (Tan *et al.*, 2002). The reluctance force was observed to be relatively small in the reference system and, therefore, has not been included in the model.

The model also takes into account the effect of

friction. Friction is very important for control engineering, for example, in the design of drive systems, high-precision servomechanisms, robots, pneumatic and hydraulic systems and anti-lock brakes for cars. Friction is highly nonlinear and may result in steady-state errors, limit cycles and poor performance (Olsson *et al.*, 1998). Friction was modeled using the simple gradient method in which the linear motor system was set in a tilted position and the moving part allowed to slide down freely. Friction was measured at several tilt angles and the results obtained were used to plot the friction function as a function of speed. The friction model took into account the Coulomb (static) and viscous (dynamic) components

$$F_{\mu} = \text{sign}(v) \left[ F_{\text{coulomb}} + \text{abs}(v) F_{\text{viscous}} \right], \quad (11)$$

where  $v$  is the velocity of the motor. The friction function was incorporated into the simulation model in such a way that it acts between the stator and the mover. In the simulation, the smoothing of the friction function was used to obtain a numerically efficient model in order to improve simulation rate. The effect of load variation was also taken into consideration. This was carried out using a forced vibrating non-homogenous two-mass model, where the load force variation  $\Delta F_l$  is calculated using a spring-mass equation, which is the sum of the spring force,  $F_s$ , and the damping force,  $F_d$ . The equation of motion for such a system is

$$\Delta F_l = F_s + F_d = k(x_1 - x_2) + c(\dot{x}_1 - \dot{x}_2) = m_2 \ddot{x}_2, \quad (12)$$

where  $k$  is the spring constant,  $c$  the damping coefficient, and  $x_i$ ,  $\dot{x}_i$  and  $\ddot{x}_i$  are the displacement, velocity and acceleration of masses  $m_i$ , respectively.

The total disturbance force equation can be described using the equations of detent force, friction force and load force variation; i.e., the disturbance force,  $F_{\text{dist}}$ , is

$$F_{\text{dist}} = F_{\text{ripple}} + F_{\mu} + \Delta F_l \quad (13)$$

This resultant disturbance force component is added to the electromotive force to influence the dynamical behavior of the linear motor system.

## 2.3 Current Controller of the Linear Motor

The current control of the system is implemented in the form of vector control. Vector control is based on the space vector theory of electrical machines and, therefore, can be easily implemented in the motor model that is also based on the space vector theory. Vector control is suitable for the force (torque) control of both induction and synchronous motors. Generally in the vector control theory, the force and flux components are analyzed separately from the motor currents using the mathematical model of the machine, and control algorithms control these components separately. In the vector control used in this study, the direct axis current,  $i_{ad}$ , is set to zero ( $i_{ad}=0$ ) assuming that it does not influence the generation of force; i.e. equation (9) transforms to

$$F_{dx} = \frac{\pi}{\tau} (\psi_d i_{aq}). \quad (14)$$

This means that angle  $\psi$ , between the armature current and q-axis, always remains at  $0^\circ$  and that the thrust is proportional to the armature current,  $i_a = i_{aq}$ . The drawback of vector control is its low robustness for changes in the machine parameters. The resistance values change considerably due to temperature variations, and the inductances rapidly reach their saturation levels. However, a vector controller is appropriate for applications in which good dynamics and/or accurate velocity control is needed.

In literature, vector control is presented in many ways. In this study, we have used a simulation principle in which the incoming thrust command,  $F^*$ , is converted to the  $i_q$  current component by dividing the force value by the force constant of the motor,  $K_m$ . The current control algorithms are executed in the rotor flux coordinates and the outputs of the controllers are transformed back into the stator reference frame, and these values,  $u_{sa}$ ,  $u_{sb}$ , and  $u_{sc}$ , are the inputs of the control inverter. In the simulation model, the modulation technique used is sinusoidal pulse width modulation (SPWM) with ideal switches.

## 2.4 Verification of the Simulation Model

The simulation model was implemented and analyzed in the MatLab/Simulink® software using the previously mentioned equations. The PWM

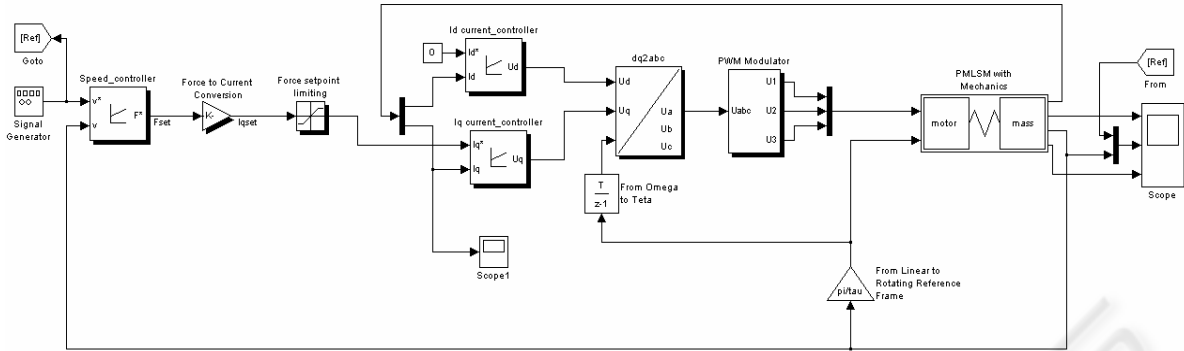


Figure 4: The Simulink model of the motor system.

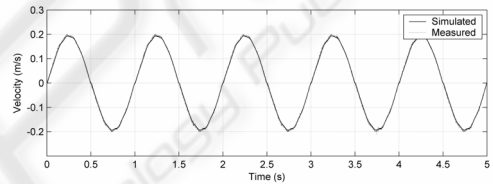
inverter is modeled as an ideal voltage source and common Simulink blocks are used for the model. The time step of the integrator in the analysis was 10  $\mu$ s, except for the velocity controller, which had a time step of 1 ms. The parameters used in the simulation are introduced in table I in the appendix. Figure 4 shows the Simulink model of the system.

The simulation results were compared with those measured in the reference system. The motor studied in this paper is a commercial three-phase linear synchronous motor application with a rated force of 675 N. The moving part is set up on an aluminum base with four recirculating roller bearing blocks on steel rails. The position of the linear motor was measured using an optical linear encoder with a resolution of approximately one micrometer. The parameters of the linear motor are given in table II in the appendix.

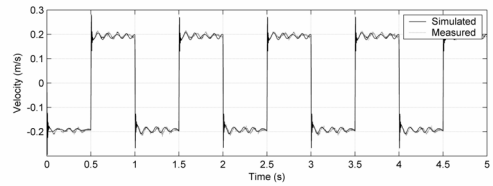
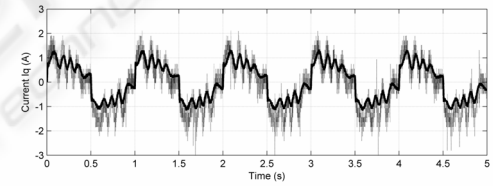
The spring-mass mechanism was built on a tool base in order to act as a flexible tool (for example, a picker that increases the level of excitation). The mechanism consists of a moving mass, which can be altered in order to change the natural frequency of the mechanism and a break spring, which is connected to the moving mass on the guide. The purpose of the mechanism is to increase the level of excitation when the motor's vibrational frequency is equal to the mechanism's natural frequency, which was calculated at being 9.1 Hz for a mass of 4 kg. The motion of the moving mass was measured using an accelerometer.

The physical linear motor application was driven in such a way that the PI velocity controller was implemented in Simulink to gain the desired velocity reference. The derived algorithm was transferred to C code for dSpace's digital signal processor (DSP) to use in real-time. The force command,  $F^*$ , was fed into the drive of the linear motor using a DS1103 I/O card. The computational time step for the velocity controller was 1 ms, while the current controller cycle was 31.25  $\mu$ s. The measured and

simulated velocity responses and force generating quadrature currents are compared in figure 5. Sine and step functions were used as the reference velocity.



(a)



(b)

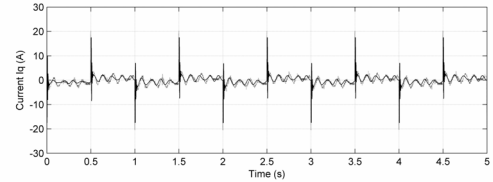


Figure 5: A comparison of the measured and simulated quadrature currents and velocity responses in the case of (a) a sine velocity reference and (b) a step velocity reference.

### 3 DISTURBANCE COMPENSATION

Disturbance compensation is applied to the motor model to reduce a detrimental force ripple. Force ripple compensation improves the speed response and robustness of the system. The force ripple, i.e. the detent force, friction, and load variation, is estimated using a disturbance observer, or in other words, a load force observer. Figure 6 shows the construction of the compensator.

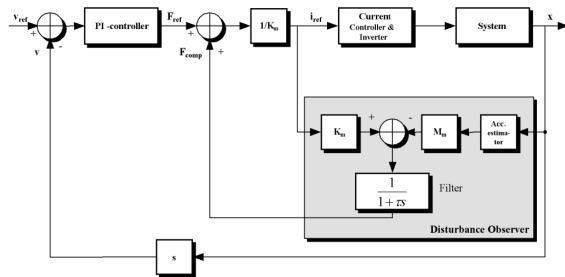


Figure 6: Disturbance compensation scheme utilizing load force estimation.

The concept of the observer is based on the comparison of the actual input force with the ideal one. This gives rise to an error, which after proper filtering, is used to produce the compensation current,  $i_{comp}$ . The filter implemented in this study is a second-order Butterworth digital low-pass filter with a cut off frequency of 50 Hz. The main function of the filter is to reduce high-frequency noise due to input signal derivation but also break the algebraic loop in the simulation model between the currents  $i_{ref}$  and  $i_{comp}$ . Unfortunately, the time delay of the filter also limits the performance of robust control, since it delays the estimated force disturbance (Godler *et al.*, 1999); therefore, the cut-off frequency should be as high as possible. Hong *et al.* (1998) suggested that an artificial delay be used in the filtering bath of the observer in order to improve dynamic behavior.

The limitations of this method are highlighted by the fact that acceleration, which is needed in the disturbance observer, is generally not available. Usually, acceleration is calculated as the time derivative of the output of the pulse encoder, although the signal becomes easily erroneous due to the high noise ratio in the encoder signal, and the filtering of this kind of signal increases the undesirable time delay, which leads to an unstable response. In this study, acceleration is estimated using an acceleration estimator, which is based on the construction introduced in (Lee *et al.*, 2001). This so-called low-acceleration estimator is based on

the fact that the displacement signal from the encoder is accurate and numerical integration provides more stable and accurate results than does numerical differentiation. Figure 7 shows the structure of the accelerated estimator.

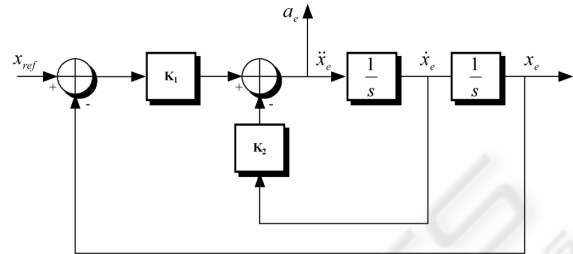


Figure 7: Structure of low-acceleration estimator.

The estimation of acceleration,  $a_e$ , is calculated from the displacement signal,  $x$ , of the encoder using a double integrator. The estimator takes the form of a PD controller, in which the estimated displacement,  $x_e$ , is set to follow the actual displacement,  $x$ ; i.e. the acceleration estimate is

$$a_e = K_1(x - x_e) - K_2 \frac{dx_e}{dt} \tag{15}$$

and the transfer function from  $x$  to  $x_e$  is

$$\frac{x_e}{x} = \frac{K_1}{s^2 + K_2s + K_1} = \frac{\omega_b^2}{s^2 + 2\zeta\omega_b s + \omega_b^2}, \tag{16}$$

where  $\omega_b$  represents the bandwidth of the acceleration estimator and  $\zeta$  is the damping ratio. Gains  $K_1$  and  $K_2$  from the PD controller can be determined from the required bandwidth of the estimator. Lee *et al.* (2001) propose that a good guideline for the damping ratio is 0.707, which corresponds to critical damping.

The proposed disturbance regulator has been tested in the simulation model introduced earlier and implemented in the physical application. The algorithm of the controller was run in real-time with a frequency of 1 kHz. The damping ratio of the acceleration estimator,  $\zeta$ , was 0.707 and the bandwidth  $\omega_b$  1000 Hz, i.e. the gains are  $K_1=10e^5$  and  $K_2=1414$ . Figure 8 shows a comparison of the velocity errors between the reference and actual velocities in compensated and non-compensated systems, when the amplitude of the reference velocity sine signal was 0.1 m/s.

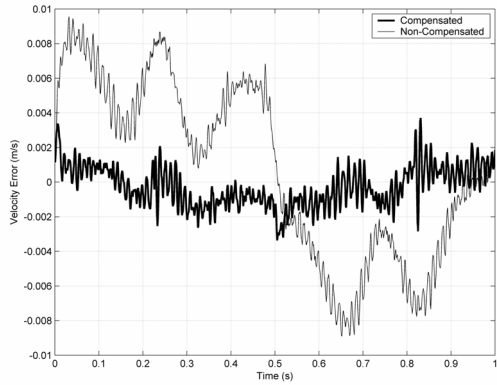


Figure 8: The error between the actual and reference velocities in the compensated and non-compensated systems, when the reference velocity signal is sine with an amplitude of 0.1 m/s.

### 4 CONCLUSION

This paper presented and verified a dynamic model for a PMLSM including non-idealities. The model appeared to be an effective tool for designing the controller of such a system. A disturbance estimator, which included a low-acceleration estimator, was proposed and successfully implemented in the control of the motor. By means of an accurate simulation model, it was possible to design and test the controller without fear of physical damage. The implementation of the proposed controller was easily carried out by using a DSP system that supported the used simulation software. Preliminary parameter tuning was performed by using the simulation model and final tuning was carried out in the physical linear motor application.

It was observed that mechanical non-idealities have important effect on the dynamics of the motor system. This effect can be reduced by constructional modifications and/or a suitable control algorithm. As mentioned before, the acceleration signal for disturbance estimation or another control algorithm is not usually available. The double derivation of the encoder signal produces a very noisy signal, and filtering this kind of signal leads to undesirable stability problems. With the proposed method, acceleration can easily be estimated from the position signal.

### APPENDIX

TABLE I  
SIMULATION PARAMETERS

Symbol	Parameter	Value
$f_N$	Nominal motor frequency	50 Hz
$\Psi_{PM}$	Magnetic flux	0.8 Wb
$L_{ad}$	D-axis armature inductance	30 mH
$L_{aq}$	Q-axis armature inductance	40 mH
$L_{md}$	D-axis magnetizing inductance	20 mH
$L_{mq}$	Q-axis magnetizing inductance	20 mH
$L_D$	D-axis damper winding inductance	30 mH
$L_Q$	Q-axis damper winding inductance	40 mH
$R$	Winding resistance	4.8 $\Omega$
$R_D$	D-axis damper winding resistance	2.4 $\Omega$
$R_Q$	Q-axis damper winding resistance	2.4 $\Omega$

TABLE II  
LINEAR MOTOR DATA BY THE MANUFACTURER

Symbol	Parameter	Value
$F_N$	Nominal force	675 N
$A_N$	Nominal current	7.2 A
$K_m$	Motor constant	94 N/A
$R_p$	Electric resistance	4.8 $\Omega$
$L_p$	Winding inductance	20 mH
$V_n$	Max. speed at nominal thrust	2.1 m/s
$\tau_M$	Pole pitch (180° electrical)	15 mm
$P_N$	Nominal power	3910 W
$L$	Stroke	1000 mm
$K_p$	P gain of vel. controller	10000 Ns/m
$K_i$	I gain of vel. controller	0.01 s
$K_p$	P gain of current controller	50.3 V/A
$K_i$	I gain of current controller	0.002 s
$f_{mod}$	Modulation frequency (PWM)	4000 Hz
$V$	Inverter bus voltage	720 V

### REFERENCES

Bassi, E., Benzi, F., Buja, G. and Moro, F., 1999. "Force disturbance compensation for an A.C. brushless linear motor," in Conf. Rec. ISIE'99, Bled, Slovenia, 1999, pp.1350-1354.

Castillo-Castaneda, E. and Okazaki, Y., 2001. "Static friction compensation approach to improve motion accuracy of machine tool linear stages," Instrumentation and development, vol. 5, no. 1, March 2001.

Chun, J.-S., Jung, H.-K. and Jung, J.-S., 2000. "Analysis of the end-effect of permanent magnet linear synchronous motor energized by partially excited primary," ICEM, International Conference on Electrical Machines, Espoo, Finland, vol. 1, pp. 333-337, 2000.

Deur, J. and Peric, N., 2000. "A Comparative study of servosystems with acceleration feedback," IEEE Ind. Applicat. Conf., Italy, 2000, pp. 1533-1540.

Godler, I., Inoue, M. and Ninomiya, T., 1999. "Robustness comparison of control schemes with disturbance

- observer and with acceleration control loop,” in Conf. Rec. ISIE'99, Slovenia, 1999, pp.1035-1040.
- Gieras, J. F. and Piech, Z. J., 2001. *Linear Synchronous Motors: Transportation and Automation Systems*. Boca Raton, USA: CRC, 2001.
- Hong, K. and Nam, K., 1998. ”A Load torque compensation scheme under the speed measurement delay,” *IEEE Trans. Ind. Electron.*, vol. 4, no. 2, April 1998.
- Hor, P. J., Zhu, Z. Q., Howe, D. and Rees-Jones, J., 1998. ”Minimization of cogging force in a linear permanent magnet motor”, *IEEE Trans. Magn.*, vol. 34, no. 5, pp. 3544-3547, Sept. 1998.
- Hyun, D.-S., Jung, I.-S., Shim, J.-H. and Yoon, S.-B., 1999. ”Analysis of forces in a short primary type permanent magnet linear synchronous motor,” *IEEE Trans. Energy Conversion*, vol. 14, no. 4, pp. 1265-1270, 1999.
- Inoue, M. and Sato, K., 2000. ”An approach to a suitable stator length for minimizing the detent force of permanent magnet linear synchronous motors,” *IEEE Trans. Magn.*, vol. 36, no. 4, pp. 1890-1893, July 2000.
- Jung, S.-Y. and Jung, H.-K., 2002. ”Reduction of force ripples in permanent magnet linear synchronous motor,” *Proceeding of International Conference on Electrical Machines*, Brugge, Belgium pp.452, Aug 2002.
- Kim, B. K., Chung, W. K. and Oh, S. R., 2002. ”Disturbance Observer Based Approach to the Design of Sliding Mode Controller for High Performance Positioning Systems,” *15th IFAC World Congress on Automatic Control*, 2002.
- Lee, S.-H. and Song, J.-B., 2001. ”Acceleration estimator for low-velocity and low-acceleration regions based on encoder position data,” *IEEE/ASME Trans. Mechatron.*, vol. 6, no. 1, March 2001.
- Morimoto, S., Sanada, M. and Takeda, Y., 1997. ”Interior Permanent Magnet Synchronous Motor for High Performance Drives,” *IEEE Trans. Ind. Applicat.*, vol. 33, Issue 4, July-Aug. 1997.
- Olsson, H., Åström, K. J., de Wit, C. C., Gäfvert, M. and Olsson, P. L., 1998. ”Friction Models and Friction Compensation,” *European Journal of Control*, 1998, Vol.4, No.3.
- Otten, G., de Vries, T.J.A., van Amorengen, J., Rankers, A.M. and Gaal, E.W., 1997. ”Linear motor motion control using a learning feedforward controller,” *IEEE/ASME Trans. Mechatron.*, vol. 2, no. 3, pp. 179-187, 1997.
- Tan, K. K., Huang, S. N. and Lee, T. H., 2002. ”Robust adaptive numerical compensation for friction and force ripple in permanent-magnet linear motors,” *IEEE Trans. Magn.*, vol. 38, no. 1, January 2002.
- Zhu, Z. Q., Xia, Z. P., Howe, D. and Mellor, P. H., 1997. ”Reduction of cogging force in slotless linear permanent magnet motors”, *Proc.IEEE Electr. Power Appl.*, vol. 144, no. 4, pp. 277-282, July 1997.